Annals of the Academy of Romanian Scientists
Series on Physics and Chemistry
ISSN 2559 – 1061 Volume 5, Number 1/2020

QUANTUM COMPUTING IN GRAPHENE

Daniela DRAGOMAN[1]

Abstract. *Quantum computing, based on different principles than classical computing, has raised high expectations regarding the increase of computational speed in nano-sized quantum systems. Therefore, the search for implementations of quantum logic gates in photons, spin states, atom/ion traps or superconducting materials, for example, is a very active research area. Graphene has demonstrated already the possibility of implementing reversible logic gates, therefore becoming a compelling candidate for quantum computing applications. The paper presents several proposals of quantum logic gates implementation in graphene, which could work at room temperature and require only current measurements as readout procedures; examples of such quantum gates are Hadamard, C-NOT, C-phase and Toffoli gates. Besides these gates, it is shown that quantum algorithms, such as the modified Deutsch-Jozsa algorithm, can be implemented also in graphene.*

Keywords: graphene, quantum computing, logic gates

1. Introduction

The motivation of searching for new computing methods is based on the fact that the impressive technological achievements in present-day computing architectures reach their limits. In particular, in order to cope with the demand of size scaling described by Moore's law, the complexity of integrated circuits must double every 18 months. Therefore, it is not possible to increase the number of transistors per processor chip beyond 2 billion MOSFET transistors without decreasing their gate length up to few tens of nanometers. As a result, MOSFETs with gate lengths of 30 nm are already in mass production, and the target of the International Technology Roadmap for Semiconductors is the fabrication of transistors with gate lengths of 7.4 nm in 2025 [1]. At such dimensions quantum effects cannot be ignored, and the alternative of quantum computation becomes enticing as well as unavoidable. The interest in quantum computers is also motivated by their predicted ability to solve in polynomial time at least some problems that have no polynomial time solution/cannot be solved in a reasonable amount of time by any classical algorithm [2]. For instance, the problem of finding the prime factors of an integer number benefits from a (sub)exponential speed-up if solved by the quantum Shor algorithm, the speed of searching of an item in an unordered list is quadratically increased by the quantum Grover algorithm, whereas simulations of

[1]Prof., Faculty of Physics, University of Bucharest, Bucharest, Romania, corresponding member of the Academy of Romanian Scientists (e-mail: daniela@solid.fizica.unibuc.ro).

the dynamics of quantum systems are expected to be performed with an exponential speed-up by quantum computers. It is therefore no wonder that an intense pursuit for physical systems that can implement quantum logic gates and algorithms is taking place nowadays. It has become clear from the beginning, however, that quantum computing can be performed only in physical systems with a small number of degrees of freedom. Among the physical systems able to implement quantum gates we mention photons, spin states, atom/ion traps and superconducting materials [3]. Because reversible logic gates have been proposed to work at room temperature in graphene [4], it is believed that this material could be employed also in quantum computing. The paper presents several proposals of quantum logic gates implementation in graphene, such as the Hadamard, C-NOT, C-phase and Toffoli gates, as well as a proposed configuration able to realize a modified Deutsch-Jozsa algorithm. Unlike other computing systems, all these graphene-based quantum gates and algorithms could work at room temperature and require only current measurements as readout procedures.

2. Physical principles of quantum computing

Classical computing is based on a succession of Boolean logic gates that operate on a bit, which can take two values: 0 and 1. In the classical quantum computer architecture based on integrated circuits, these two logic values are usually encoded in the voltage state of field-effect transistors, 0 corresponding to a low voltage state and 1 to a high voltage, as shown in Figure 1, a. When the voltage has an intermediary value between those associated to the 0 and 1 logic states, an error occurs in classical computing.

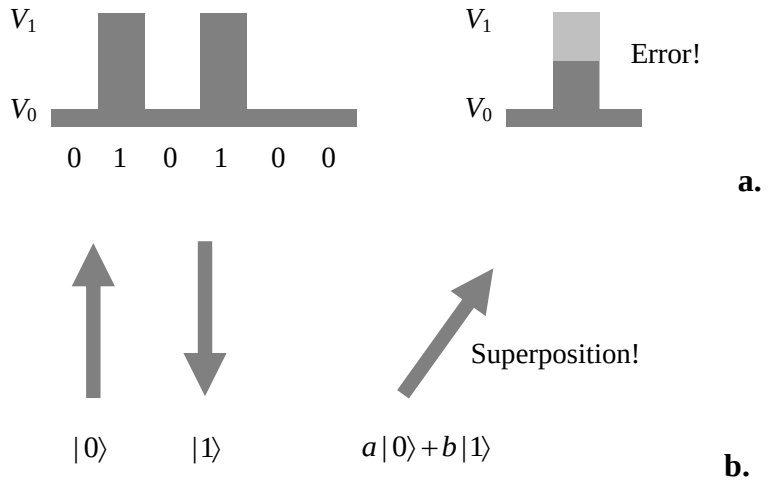

Fig. 1. a. Classical bits encoded in voltage values of a transistor, and **b.** quantum qubits encoded in spin orientation.

On the other hand, a quantum bit, or qubit, can be encoded in any two-state quantum systems. For example, as illustrated in Figure 1, b, the logical $|0\rangle$ and $|1\rangle$ states (the basis states) can be encoded in the spin-up and spin-down eigenstates of a spin-1/2 particle. However, the intermediary state $a|0\rangle + b|1\rangle$ is no longer interpreted as an error, but as a linear superposition of spin-up and spin-down eigenstates with generally complex coefficients *a* and *b*, the square of the absolute values of which represent the probability of realizing the respective eigenstate. As such, the following relation must be satisfied: $|a|^2 + |b|^2 = 1$.

The possibility of implementing superposition states in quantum physical systems changes the way in which computation is performed. More precisely, whereas an *n*-bit classical register (string of bits) can store only one of the possible 2^n encoded states, which is then subjected to a sequence of logic gates before it delivers the result of a computation, an *n*-qubit register stores a superposition of the 2^n possible states, which are subjected to various interactions in parallel, and evolves into a final state, which can itself be a superposition. Although parallel computation can be performed also with classical computers, it implies synchronized operation of multiple computing machines, whereas parallel computing is an inherent feature of any quantum computer.

The intrinsic quantum parallelism is responsible for the computational speed-up, but it also implies that any inquiring of the state of a qubit, i.e. any measurement, can be performed without disturbing the result only after the algorithm is completed. Even then, a single read-out of the result is possible only if the output state of the qubit is in one of the basis states $|0\rangle$ and $|1\rangle$. This consequence of quantum mechanics makes the design of quantum algorithms more involved than classical algorithms, where no such precautions are necessary because the voltage state of a transistor can be measured at any time (even during computation) without interfering with the outcome.

Quantum superposition is responsible also for other important differences between classical and quantum computing. For instance, unknown qubits cannot be cloned [5] while classical bits can be easily copied, whereas qubit entanglement, with no classical analog, can be used in designing efficient algorithms. This suggests that classical and quantum logic operations/gates are also different, and that there are quantum gates with no classical counterpart. Indeed, while classical logic gates are Boolean operators and algorithms usually employ irreversible fan-out gates and disposable ancilla (work bits), quantum gates are implemented with unitary and reversible operators.

Quantum gates can be represented by matrices acting on qubits that can be expressed as vectors. If the superposition state is written as:

$$a|0\rangle + b|1\rangle = \begin{pmatrix} a \\ b \end{pmatrix} \tag{1}$$

the action of a NOT gate (also denoted as X gate in quantum computing), for example, which interchanges the to logic states can be expressed as

$$U_{NOT} = X = \begin{pmatrix} 0 & 1 \\ 1 & 0 \end{pmatrix}. \tag{2}$$

Whether the NOT operator is also encountered in classical computing, and can be represented by the same matrix, the Hamadard gate, the matrix of which is

$$H = \sqrt{U_{NOT}} = \frac{1}{\sqrt{2}} \begin{pmatrix} 1 & 1 \\ 1 & -1 \end{pmatrix} \tag{3}$$

has no classical counterpart because it transforms a basis state $|0\rangle$ and $|1\rangle$ into a superposition. The Z operator, which changes the sign (phase) of the $|1\rangle$ state, has also no classical analog, since classical bits have no sign. The corresponding matrix of the Z operator is

$$Z = \begin{pmatrix} 1 & 0 \\ 0 & -1 \end{pmatrix}. \tag{4}$$

Quantum computing cannot be implemented without conditional gates, i.e. gates in which the state of one qubit, the target qubit, is change in a prescribed manner only if another quantum state has a definite value. The simplest conditional gates act on a 2-qubit state/register, which can be written as

$$a|00\rangle + b|01\rangle + c|10\rangle + d|11\rangle = \begin{pmatrix} a \\ b \\ c \\ d \end{pmatrix} \tag{5}$$

where $|xy\rangle = |x\rangle \otimes |y\rangle$, x, y = 0, 1, represent the state in which the first qubit has the logical value $|x\rangle$ and the second one the logical value $|y\rangle$. For instance, the CNOT (controlled NOT) gate, which performs a NOT operation on the second, target qubit, when the first, control qubit is in the state $|1\rangle$, can be represented by

$$U_{CNOT} = \begin{pmatrix} 1 & 0 & 0 & 0 \\ 0 & 1 & 0 & 0 \\ 0 & 0 & 0 & 1 \\ 0 & 0 & 1 & 0 \end{pmatrix} \tag{6}$$

while the matrix of the C-phase (controlled phase) gate, which changes the phase of the second/target qubit when it has the logic value $|1\rangle$ if the first/control qubit is $|1\rangle$, is

$$U_{Cph}(\phi) = \begin{pmatrix} 1 & 0 & 0 & 0 \\ 0 & 1 & 0 & 0 \\ 0 & 0 & 1 & 0 \\ 0 & 0 & 0 & \exp(i\phi) \end{pmatrix} \tag{7}$$

In addition, 3-qubit gates, such as CCNOT, or Toffoli gate, can be defined, which apply the NOT operation on a target qubit only if the logic states of two control qubits are $|1\rangle$. The CNOT gate, together with one-qubit gates form the set of universal logic gates in quantum computing, whereas the corresponding set in classical computing contains only one gate: NAND or NOR.

3. Physical systems for quantum computing implementation

As already mentioned, any quantum system with exactly two states, which can be associated to the logic states $|0\rangle$ and $|1\rangle$, can implement a qubit. To build a quantum computer, a scalable physical system with well defined qubits is required, it should be possible to initialize the qubits to a desired state and to control the interaction between qubits in order to implement conditional quantum logic gates, and qubit-specific measurement capabilities are compulsory. In addition, long decoherence times are needed, since loss of coherence of a quantum state due to interaction with the environment leads to errors. These requirements are not easily satisfied. In particular, the decoherence time is generally below 0.1 s, which implies that the number of quantum operations that can be performed before decoherence sets in is about 10^{13} at most, whereas a classical computer performs 5×10^{10} operations/s with no decoherence-related limitations of the operating time. Moreover, there are still technical difficulties regarding the implementation and control of many-qubit states. In fact, present-day classical computers are so performant that they could be surpassed only by quantum computers operating on about 40-qubit registers.

Despite these considerations, there are attempts to implement qubits and quantum logic gates in many physical systems, including ensembles of molecules, photons, spin states, trapped atoms or ions, superconducting materials, etc. Ensemble of

molecules, usually in solution, can implement qubits by encoding them in the spin state of component atoms, for instance in the spin of ^{13}C in α-D-methylglucose and of ^{19}F in 4-bromo-1,1,2-trifluoro-1-butene in solution [6]. Then, the dimension of the quantum register consisting of such NMR qubits is limited to the number of spin states in the molecule. Each qubit can be individually addressed since their resonance frequencies are slightly different due to different neighborhoods, and the interaction between qubits, necessary for implementing conditional gates, is governed by nuclear spin-spin coupling in NMR. Despite the virtual impossibility of preparing a pure state of spins at thermal equilibrium (only pseudo-pure states can be obtained above 1 mK by spin alignment in magnetic fields), several 2-qubit and 3-qubit logic gates have been demonstrated [6], and even a quantum Fourier transform algorithm was shown to successfully work on a periodic 3-qubit system, the qubits being encoded in ^{13}C spins of alanine [7]. However, the computing accuracy of NMR qubits is not high enough for a reliable computer, the quantum Fourier transform algorithm, for example, being implemented with an accuracy of 80%.

Photon qubits have received particular attention due to the extremely long decoherence time. The qubits are generally encoded in the polarization states (horizontal or vertical) of photons, and simple optical elements such as polarizing beam splitters and half-wave plates can be used to initialize quantum states and to implement quantum gates. Moreover, photon qubits can be transported at large distances using optical fibers. The configurations used for implementing several quantum gates with this type of qubits, as well as their accuracies, are reviewed in [8]. Presently, photonic qubits are mainly used in quantum cryptography, especially in quantum key distributions over large distances. Successful experiments on long-distance (over 100 km) high-rate (up to 27.6 bps) quantum key distribution have been reported in [9], while teleportation experiments over 100 km of optical fiber with an average fidelity of about 84%, and over free-space channels between the 143-km-separated Canary islands of La Palma and Tenerife have been demonstrated in [10] and [11], respectively. There are currently several quantum key distribution networks in use by institutions (for example, DARPA) and metropolitan areas (Geneva and Tokyo). Moreover, companies such as SeCureNet (Paris), MagiQ Technologies (New York), ID Quantique (Geneva) and QuintessenceLabs (Australia) are offering commercial systems for quantum key distribution [12].

Implementations of quantum gates in solid state systems constitute an active area of research due to an increased possibility of control and manipulation compared to NMR qubits. Several configurations have been proposed and realized, all of them working at low temperatures. For instance, qubits could be encoded in the nuclear spins of donor impurities, such as ^{31}P atoms in Si [13], several quantum

gates at 50 mK being demonstrated in [14]; the decoherence time, of 8 μs, limited the operation to a number of 100 2-qubit gates. Qubits can be encoded also in the charge of coupled quantum dots, the initialization of the quantum state being controlled by voltages applied on gate electrodes [15]; the decoherence and gate times in this case were found to be about 4 ns and 50 ps, respectively.

Large decoherence times and quantum registers are expected in trapped atoms or ions. Indeed, it was shown that different logic gates, with an average fidelity of 95%, can be simultaneously performed at adjacent sites of an optical lattice with a period of 426 nm that traps Cs atoms with a density of 1 atom/100 sites [16]. The experimental set-up, technical difficulties and sources of errors in the implementation of quantum logic gates using trapped ions are briefly discussed in [17], where results of several quantum gates, including the quantum Fourier transform, on trapped $^{40}Ca^{+}$ ions are also presented. The decoherence time is in this case 15 ms, but the gate duration is comparable, of about 2 ms, and the fidelity of logic gates varies between 72% and 81%. Recently, nitrogen vacancies in diamond nanocavities showed promising preliminary results for spin-based quantum computing [18].

By far, the most successful quantum system for implementing logic operations is the superconducting circuit. In this macroscopic system, qubits can be encoded in several variables and can be manipulated by electromagnetic pulses and/or applied voltages. Flux qubits, charge qubits or phase qubits can be encoded in the direction of the flux/superconducting current around a loop interrupted by one or three Josephson junctions, the number of Cooper pairs in a small superconducting island connected to a voltage source via a capacitor and a Josephson junction and, respectively, the energy levels in an anharmonic potential well that forms in a single current-biased Josephson junction [19]. A recent review of the performances of superconducting qubit operations can be found in [20]. Despite the technological challenges imposed by the necessity of operating below the critical temperature, of up to some tens of mK, a number of over 100,000 operations can be performed on such quantum computers until decoherence sets in. In fact, superconductive qubits have led to the development of the first commercial quantum computer, called D-Wave. The D-Wave Systems company, launched the first 128-qubit computer, D-Wave One, in 2011, the 512-qubit D-Wave Two system in 2013 and the 1000+ qubit D-Wave 2X computer in 2015, in collaboration with NASA and Google [21]. Superconducting qubits caught also the attention of IBM, which reported the fabrication of a 4-qubit chip able to detect and correct quantum computing errors [22], while quantum supremacy has been claimed by the Sycamore programmable superconducting processor [23].

In summary, there is a forceful on-going race for the development of quantum computing strategies that will be able to compete with and overcome the present-

day classical computers. Whether quantum computers are much faster in solving at least some problems, no quantum architecture can compare in price and widespread use with our laptops. As such, any solution for a cheaper and room-temperature technology for implementing quantum logic gates and algorithms are of great interest. In this respect, nanomaterials could be a viable alternative.

4. Quantum computing implementation in graphene

Graphene demonstrated already the possibility to miniaturize reversible logic gates by using new configurations [4]. Reversible logic gates have, ideally, no power loss. By associating logical irreversibility, i.e. the non-uniqueness relation between input and output, with physical irreversibility, a minimum heat of $\ln(2k_BT)$ per erased bit/information loss is expected to be dissipated during operation [24]. Although this is not the only source of heat dissipation, it is a source that cannot be avoided in irreversible computing. Therefore, reversible logic could be a solution to minimize the heat problem. Implementing reversible logic gates, such as the 3-bit Toffoli gate, is not easy in the MOSFET technology, as can be seen from the layout of this gate in [25].

By using common nanomaterials, reversible logic gates could be miniaturized. However, a dramatic simplification of these gates can be achieved only via a drastic change in their architecture. Graphene offered the possibility to modify the layout of a Toffoli gate because of its unique electronic bandstructure [26]. Its specific periodic arrangement of carbon atoms in a one-atom thick hexagonal lattice leads to a particular linear dispersion relation in the neighborhood of the unequivalent corners K and K' of the hexagonal first Brillouin zone, denoted as Dirac points. This property, together with the fact that charge carriers in graphene obey a massless Dirac-like equation, the two components of the spinors corresponding to the contributions of the two triangular sub-lattices of the crystalline structure of graphene, renders graphene different from common semiconductor, described by the Schrödinger equation and a parabolic dispersion relation. As such, specific phenomena are expected to occur in graphene. In particular, it was shown both theoretically [27] and experimentally [28] that electrostatic potentials cannot modulate the transmission of normally incident electrons or holes, unless these are applied on oblique gates. Then, a succession of two or three individually biased oblique gates can implement reversible logic operations, such as CNOT and CCNOT, respectively [4]. An implementation of a CCNOT (Toffoli) gate by just three oblique gates is indeed a dramatic simplification of the layout of this gate compared to that in [25].

However, oblique gates cannot implement qubits, at least not when the logic gates are encoded by gate voltages, as in [4]. The reason is that superposition states cannot be created in this way. Therefore, another solution is needed. As

demonstrated theoretically in [29] and experimentally in [30], a Y-junction can implement a controllable superposition state, the logical states $|0\rangle$ and $|1\rangle$ being encoded in the wavefunctions propagating along the two emerging arms of the junction. In a symmetric Y-junction, the generated state is $(|0\rangle+|1\rangle)/\sqrt{2}$, but transverse electric fields in the splitting region can tune the superposition [29, 30].

By encoding the $|0\rangle$ and $|1\rangle$ states of the input qubit *in* the wavefunctions propagating along the two arms of a symmetrical Y junction in graphene (see Figure 2, a), it is possible to implement a one-qubit operation, such as a Hadamard gate, if the two arms interfere in a wider region [31]. The output qubit *out* can be seen also as a symmetrical Y-junction, the outgoing arms being denoted by *out*1 and *out*2.

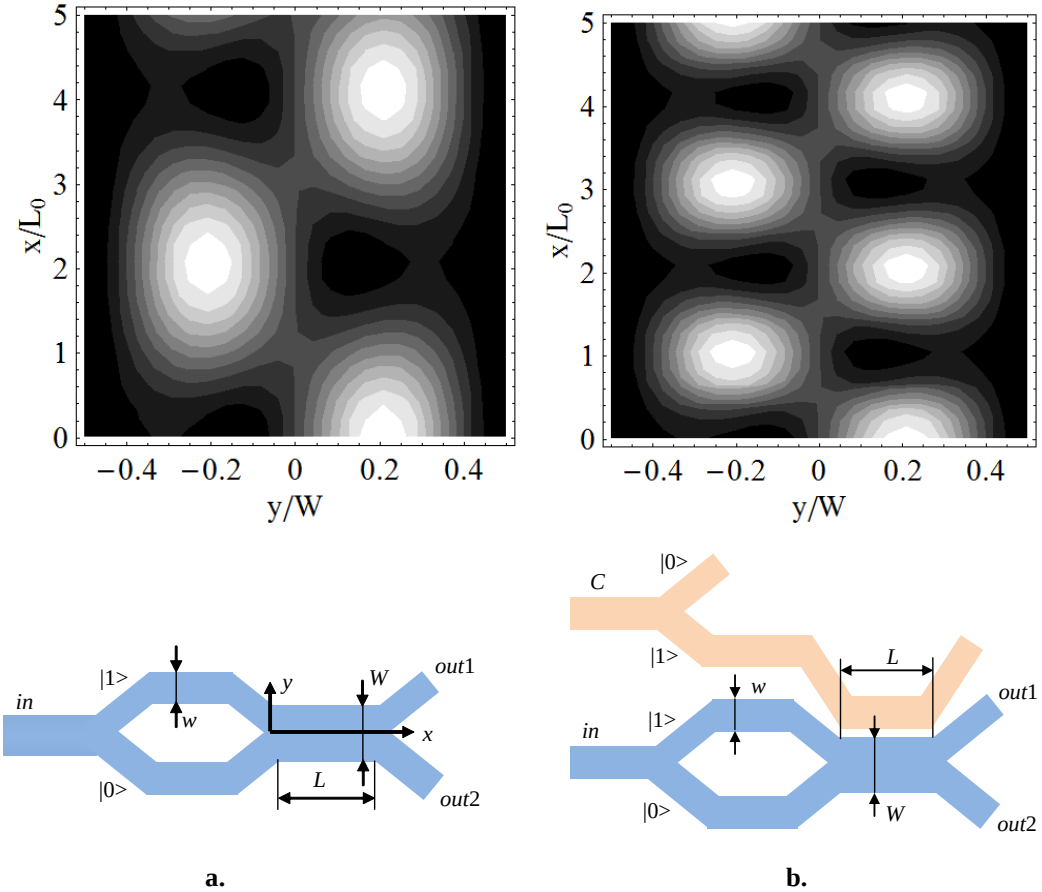

Fig. 2. Evolution of the probability distribution (top) in the interference region and the corresponding configuration in graphene (bottom) of **a.** a Hadamard gate and **b.** a CNOT gate

The probability distribution function evolution of electrons in the interference region when $in = |1\rangle$ is shown in Figure 2, a, the simulations being performed for widths of the Y-junction arms, denoted by *w*, small enough such that only one mode, with propagation constant $k = [(E/\hbar v_F)^2 - (\pi/w)^2]^{1/2}$ is allowed, whereas in the wider interference region, of width *W*, two modes with propagation constant $k_m = [(E/\hbar v_F)^2 - (m\pi/W)^2]^{1/2}$, *m* = 1, 2 can exist. The number of modes in a waveguide with width *d* is given by the integer part of $Ed/(\pi\hbar v_F)$. Here *E* is the electron energy, and v_F = 10^6 m/s is the Fermi velocity. In particular, the simulations were made for *W* = 80 nm, $w = W/2$ = 40 nm, *E* = E_0 = 65 meV, the propagation length being normalized to L_0 = 50 nm.

As seen from Figure 2, a, where (as in the rest of the paper) darker colors correspond to smaller probability values, when *L* = $L_H = 1.03\,L_0$, the transmission probability/electrical currents in *out*1 and *out*2 are equal, as in a Hadamard gate. On the other hand, when $L = 2L_H \cong 2.06L_0$, the input logic state $|1\rangle$ transforms into $|0\rangle$, i.e. a NOT gate is implemented if the output states are identified with *out*2 = $|0\rangle$ and *out*1 = $|1\rangle$. Similarly, when $L = 4L_H \cong 4.12L_0$ the probability distribution/input state remains unchanged, as in the Identity operation [31].

Conditional/controlled logic gates can also be implemented in graphene [31]. For instance, the two-qubit CNOT gate can be implemented in graphene by the configuration represented in Figure 2, b, the control qubit *C* influencing the result of interference in the wider region only when it is equal to $|1\rangle$. As this interference pattern is determined by the phase difference between the two propagating modes in the wider region of length *L* and wide *W*, given by

$$\Delta\phi(E,L) = L\left[\sqrt{(E/\hbar v_F)^2 - (2\pi/W)^2} - \sqrt{(E/\hbar v_F)^2 - (\pi/W)^2}\right], \qquad (8)$$

it follows that the control-target qubits' Coulomb interaction, modeled as a potential energy *V* applied on the entire length of the interference region, modifies the interference pattern in this region by affecting the Fermi energy level of charge carriers. In particular, a CNOT gate is implemented for a potential energy *V* for which $\Delta\phi(E,2L) = \Delta\phi(E-V,L)$. In this case, choosing *L* such that in the absence of the interaction the gate implements the Identity operation, when the interaction is present, it implements the NOT operation. Actually, the length of the gate can be halved if the logical values of the outputs *out*1 and *out*2 are identified with $|0\rangle$ and $|1\rangle$, respectively, case in which the gate implements the Identity operation for $L = 2L_H \cong 2.06L_0$ only. For the same values of the simulation parameters as above, CNOT is obtained for a potential *V* = 13.2 meV.

The evolution of the probability distribution in the interference region for this value of V is represented in Figure 2, b.

In an analogous way, the graphene-based configuration in Figure 3, a is a two-qubit C-phase gate provided that the nanoribbons associated to the $|1\rangle$ states of the input *in* and controlled qubits *C* interact/are in close proximity over a length L. The Coulomb interaction between charge carriers in the two nanoribbons can be modeled as a potential energy V, which influences the interference pattern in the region of width W. More precisely, V increase the phase of the $|1\rangle$ state of the *in* qubit with respect to the $|0\rangle$ state of the same qubit with an additional amount

$$\Delta\varphi = L\left[\sqrt{(E-V)^2/(\hbar v_F)^2-(\pi/w)^2}-\sqrt{(E/\hbar v_F)^2-(\pi/w)^2}\right], \qquad (9)$$

only when the control qubit has the logical value $|1\rangle$. When the state of C is $|0\rangle$, the input/target and control qubits do not interact, so that the state of the first one is unchanged. If the interaction length is $L = L_0$ and the electron energy equals E_0, $\Delta\varphi$ varies between 1.13 rad and -1.55 rad as V changes from -10 meV to 10 meV, and vanishes for $V = 0$.

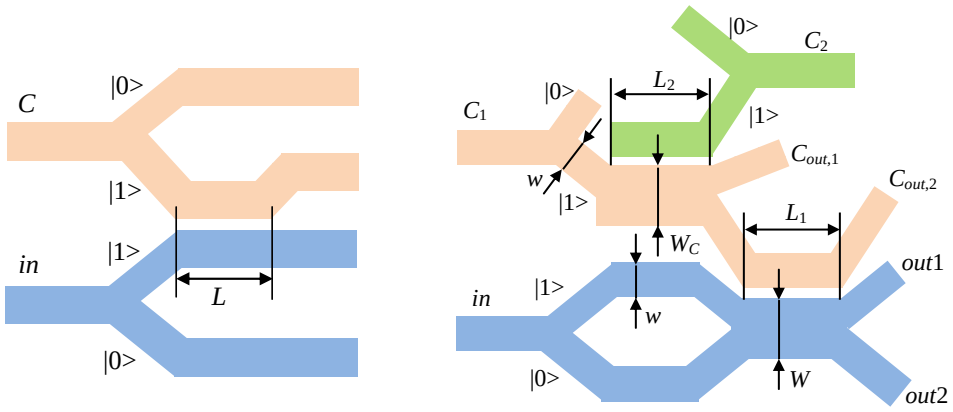

a. **b.**

Fig. 3. Schematic representations of configurations implementing **a.** a qubit C-phase and **b.** a Toffoli gate in graphene.

Based on the previous results, the proposed graphene-based configuration for implementing the universal three-qubit Toffoli logical gate looks like that in Figure 3, b. In this case, the nanoribbons *out*1 and *out*2 must exchange their logical values only when both C_1 and C_2 are $|1\rangle$, i.e. when ballistic electrons in the arm of C_1 associated to $|1\rangle$ interact with C_2 = $|1\rangle$ such that the electrons emerge from the control interference region of width W_C through the bottom

nanoribbon, $C_{out,2}$. Assuming that $W_C = W$, and the values of all other parameters are the same as above, the previous condition is fulfilled when $L_1 = L_2 \cong 2.06 L_0$.

5. Graphene-based implementation of a modified Deutsch-Jozsa algorithm

Quantum algorithms can be implemented as succession of quantum gates, in particular as successions of universal Toffoli gates. However, it would be desirable if simplified configurations would be found for solving particular problems. In this section we show that a modified Deutsch-Jozsa (DJ) algorithm can be implemented in graphene.

The original quantum DJ algorithm [32] determines if a Boolean function, which can be defined on one or few qubit states, is constant or balanced, without knowing the values of the function on the input states. By definition, a balanced function takes the output value $|0\rangle$ on exactly one half of the basis input states and the output value $|1\rangle$ on the other half. In practical applications, a modified version of the DJ algorithm, which determines whether an arbitrary function (not necessarily Boolean) defined on one or few qubit states is constant or not, would be of greater interest [33]. The reason is that the function referred to in this context can represent an interaction described by a Hamiltonian. As in the original DJ algorithm, the answer to the question whether the interaction is constant or not is found without estimating/measuring the interaction results; only the overall symmetry properties of the interaction potential matter.

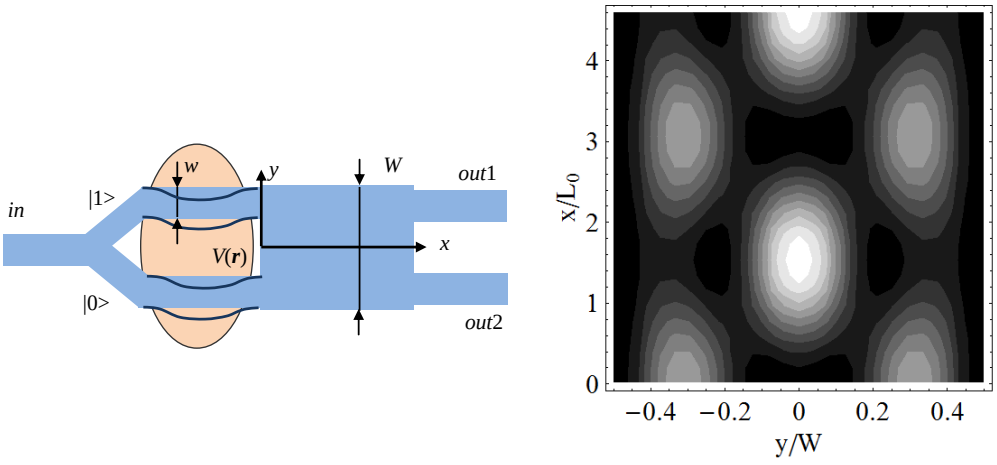

a. **b.**

Fig. 4. a. Graphene-based configuration implementing the 1-qubit modified DJ algorithm, and **b.** the quantum probability distribution evolution in the interference region for identical incoming wavefunctions in the lower and upper arms

The modified DJ algorithm described above with a 1-qubit input state can be implemented with the graphene-based configuration in Figure 4, a [33]; the generalization of this configuration for 2-qubit states is discussed in detail in [33]. As in all quantum gates presented in the previous section, the input qubit *in* is a symmetric graphene-based Y junction with output arms of width *w* that support only one mode, the $|0\rangle$ and $|1\rangle$ quantum logic states interacting then with a potential $V(\boldsymbol{r})$ along a certain length. The device in Figure 4, a, determines whether $V(\boldsymbol{r})$ is constant or not, i.e. has a uniform or non-uniform spatial distribution, by allowing the quantum wavefunctions after interaction to interfere in a wider region of width *W*. If, as a result of the interaction, both wavefunctions are affected in the same (unknown) way, the outgoing wavefunctions, propagating in the symmetrically placed nanoribbons *out*1 and *out*2 are identical/symmetric, and the currents measured in the *out*1 and *out*2 leads have the same value. Otherwise, the output currents will be different. In fact, in order to definitely decide between a constant potential energy distribution and a symmetric one with respect to the *y* axis, the nanoribbons in the interacting region should have the form suggested by the dark blue lines in Figure 4, a.

For a better understanding of the working principle of the device above, Figure 4, b shows the evolution of the quantum probability distribution in the interference region when the wavefunction entering this region by the lower arm is identical to that in the upper arm; the interference pattern is in this case symmetric with respect to the $y = 0$ axis, as are the wavefunctions collected by symmetric outgoing nanoribbons, such that the currents in *out*1 and *out*2 are identical. On the contrary, if the wavefunction entering the interference region by the lower arm differs from that in the upper arm by an amplitude factor $a = 1.5$ or a phase difference of $\phi = \pi/6$, the corresponding interference patterns/evolutions of the quantum probability distribution, displayed in Figures 5, a and b, respectively, are no longer symmetric with respect to the $y = 0$ axis, and the *out*1 and *out*2 are different. Similar differences are found for any difference in amplitude or phase between the wavefunctions entering the interference region. The simulations were performed for $w = 40$ nm, $W = 120$ nm, $E_0 = 60$ meV, the propagating length being normalized to $L_0 = 50$ nm; for these parameters the arms of the Y-junction support only one mode, whereas the interference region supports 3 modes.

Because the ratio of two currents can be measured with a typical error of 2%, the decision whether $V(\boldsymbol{r})$ is a constant function is in fact taken if the ratio of the *out*1 and *out*2 currents is between 0.98 and 1.02. This error, which limits the sensitivity of the device, can lead to incorrect decisions about the spatial symmetry of $V(\boldsymbol{r})$. However, for poperly designed devices, measurements of *out*1 and *out*2 currents can determine the spatial symmetry of the potential energy for a

considerable range of a and ϕ values. This range can be further narrowed by using advanced equipments that reduce significantly the current measurements errors.

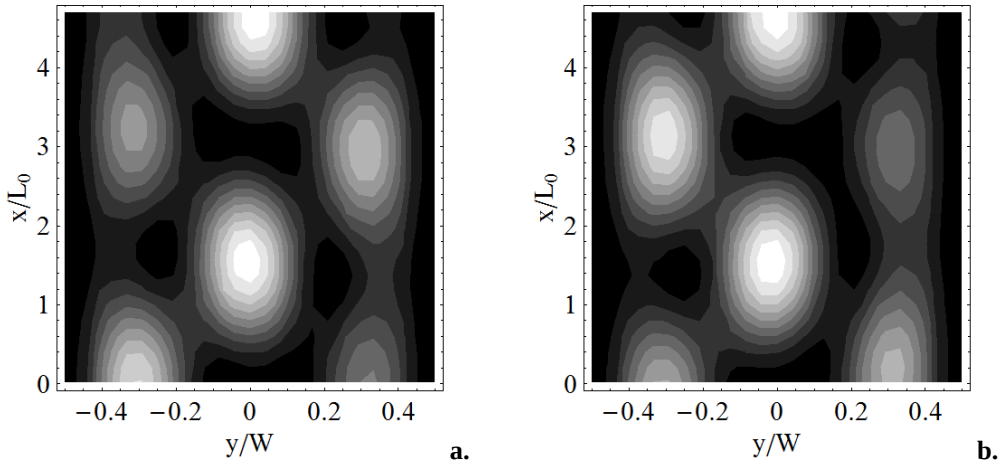

Fig. 5. Probability distribution evolution in the interference region of the device in Figure 4, a when the incoming wavefunction in the lower arm **a.** has an amplitude 1.5 times larger than in the upper arm, and **b.** has a phase difference of $\pi/6$ with respect to the upper-arm wavefunction.

Conclusions

After a brief description of quantum computing principles and a short overview of physical systems that can implement quantum logic gates, graphene-based configurations were shown to realize Hadamard, C-phase, CNOT, and Toffoli quantum logic gates, as well as a modified quantum DJ algorithm. Other algorithms could be implemented as successions of the above-mentioned quantum gates, the total length of such configurations being required to be smaller than the phase-coherence length in order to avoid decoherence. Besides being miniaturized, the main advantage of quantum computing in graphene nanoribbons is that the phase-coherent transport regime of charge carriers, indispensable for quantum computing, is maintained over large distances even at room temperature. Indeed, the measured mean-free path, i.e. the average distance between collisions, of graphene deposited on SiO_2 is about 400 nm at room temperature, increases up to 1 μm if graphene is encapsulated in boron nitride monolayers [34], and is longer than 10 μm for graphene nanoribbons of similar widths as those considered in this paper, epitaxially grown on SiC [35]. Phase-coherence lengths are longer than mean-free paths since coherence is lost due to scattering, therefore the maximum lengths of graphene-based computing devices could be several times longer than the mean-free path values given above [36, 37].

The large room-temperature phase-coherence length of graphene is the foremost advantage of this material, no other known materials being characterized by

comparable mean-free path values, except at very low temperatures. In addition, the quantum gates and the proposed modified DJ algorithm can be patterned currently on CVD grown graphene flakes at 4-inch and 6-inch wafer scale with the existing nanotechnologies of a standard clean room. Thus, graphene-based quantum computers could be commercially available in the near future.

Recently, graphene-based configurations similar to those studied above have been fabricated at the wafer scale and showed (quasi-)ballistic transport at room temperature [38]. Preliminary studies show that these configurations could be used to implement one-qubit quantum gates or the one-qubit modified DJ algorithm.

R E F E R E N C E S

[1] F. Schwierz, Nature Nanotechnol. **5**, 487 (2010).

[2] M. A. Nielsen and I. L. Chuang, *Quantum Computation and Quantum Information*, 10th edition (Cambridge Univ. Press, Cambridge, 2011).

[3] T. D. Ladd *et al.*, Nature **464**, 45 (2010).

[4] D. Dragoman and M. Dragoman, Appl. Phys. Lett. **105**, 113109 (2014).

[5] W. K. Wootters and W. H. Zurek, Nature **299**, 802 (1982).

[6] D. Golze *et al.*, Concepts Magn. Reson. Part A **40A**, 25 (2012).

[7] Y. S. Weinstein *et al.*, Phys. Rev. Lett. **86**, 1889 (2001).

[8] P. Kok *et al.*, Rev. Mod. Phys. **79**, 135 (2007).

[9] K. Takemoto *et al.*, Sci. Rep. **5**, 14383(2015).

[10] H. Takesue *et al.*, Optica **2**, 832 (2015).

[11] X.-S. Ma *et al.*, Nature **489**, 269 (2012).

[12] https://en.wikipedia.org/wiki/Quantum_key_distribution

[13] B. E. Kane, Nature **393**, 133 (1998).

[14] M. Veldhorst *et al.*, Nature **526**, 410 (2015).

[15] G. Cao *et al.*, Nature Commun. **4**, 1401 (2013).

[16] J. H. Lee *et al.*, Nature Commun. **4**, 2017 (2013).

[17] P. Schindler *et al.*, New J. Physics **15**, 123012 (2013).

[18] R.E. Evans et al., Science 362, 662 (2018).

[19] J. Clarke and F. K. Wilhelm, Nature **453**, 1031 (2008).

[20] M. H. Devoret and R. J. Schoelkopf, Science **339**, 1169 (2013).

[21] http://www.dwavesys.com

[22] A. D. Corcoles *et al.*, Nature Commun. **6**, 6979 (2015).

[23] F. Arute et al., Nature **574**, 505 (2019).

[24] R. Landauer, IBM J. Res. Develop. **5**, 183 (1961).

[25] http://www.diku.dk/forskning/Publikationer/tekniske_rapporter/2012

[26] A.H. Castro Neto *et al.*, Rev. Mod. Phys. **81**, 109 (2009).

[27] D. Dragoman and M. Dragoman, Appl. Phys. Lett. **90**, 143111 (2007) .

[28] M. Dragoman *et al.*, Nanotechnology **25**, 415201 (2014).

[29] Th. Palm and L. Thylén, Appl. Phys. Lett. **60**, 237 (1992).

[30] G.M. Jones *et al.*, Appl. Phys. Lett. **86**, 073117 (2005).

[31] D. Dragoman and M. Dragoman, J. Appl. Phys. **119**, 094902 (2016).

[32] D. Deutsch and R. Jozsa, Proc. Roy. Soc. London A **439**, 553 (1992).

[33] D. Dragoman and M. Dragoman, Nanotechnology **26**, 485201 (2015).

[34] A.S. Mayorov *et al.*, Nano Lett. **11**, 2396 (2011).

[35] J. Baringhaus *et al.*, Nature **506**, 349 (2014).

[36] J. Berezovsky *et al.*, Nanotechnology **21**, 274013 (2010).

[37] A.A. Kozikov *et al.*, Phys. Rev. B **86**, 045436 (2012).

[38] M. Dragoman *et al*., IEEE Trans. Nanotechnol. **17**, 362 (2018).